Morphodynamic modeling the impact of large-scale embankment on the large bar in a convergent estuary

Xie, Dongfeng; Wang, Zheng Bing ; van der Wegen, Mick; Huang, Junbao

DOI
10.1016/j.margeo.2021.106638

Publication date
2021

Document Version
Accepted author manuscript

Published in
Marine Geology

Citation (APA)
Xie, D., Wang, Z. B., van der Wegen, M., & Huang, J. (2021). Morphodynamic modeling the impact of large-scale embankment on the large bar in a convergent estuary. *Marine Geology*, *442*, Article 106638. https://doi.org/10.1016/j.margeo.2021.106638

Morphodynamic modeling the impact of large-scale embankment on the large bar in a convergent estuary

Dongfeng Xie[a], Zheng Bing Wang[b,c], Mick Van der Wegen[c,d], Junbao Huang[a]

[a]Zhejiang Institute of Hydraulics and Estuary, Hangzhou, China; Zhejiang Provincial Key Laboratory for Estuarine and Coastal Research, China

[b]Faculty of Civil Engineering and Geosciences, Delft University of Technology, The Netherlands

[c]Deltares, P.O. Box 177, 2600 MH Delft, The Netherlands

[d]IHE Delft, PO Box 3015, 2601 DA Delft, the Netherlands

Corresponding author: Dongfeng Xie (dongfeng.xie@hotmail.com).

Abstract: Many alluvial estuaries worldwide include an inside bar system, a large sediment deposit deeply stretched into the estuary. A good example of such a system is the large sediment deposit in the Qiantang Estuary, China. Its length and height reach 130 km and 10 m, respectively. Bathymetrical comparison reveals that the large bar has moved seaward by around 15 km over the last decades, probably related to the large-scale coastal embankment project. This motivated a quantitative investigation of the impact of estuarine planform on the inside bar development. The bar morphology is reproduced by means of an idealized 1-D morphodynamic model. Model results suggest that the bar movement is related to a decreasing tidal prism, increasing flood dominance in the lower reach and enhanced ebb currents in the upper reach, in response to the embankment. The timescale of the morphological response is only several years. The rapid response is related to the strong tidal currents and large sediment fluxes within the estuary. Sensitivity experiments show

that the location and dimensions of the bar are related to the convergence length of the estuary. A decrease of the convergence length causes seaward movement and shortening and lowering of the bar. The bar dimensions also depend on the ratio between river and tidal discharges. When the ratio increases, the bar apex moves seaward and the elevation decreases. The bar movement has significantly influenced the tidal bore in the Qiantang Estuary.

Keywords: morphodynamic modeling; inside bar dimensions; coastal embankment; tidal bore; Qiantang Estuary; coastal management

1. Introduction

Located at the transitional zone between river and the sea, estuaries are of enormous societal and environmental importance. They provide accessibility for navigation, freshwater and fertile soil of the adjacent floodplains. Therefore most densely populated areas of the world are situated near estuaries. Estuaries also play an important role in global carbon/biogeochemical cycling, and serve as a crucial feeding and breeding ground for various flora and fauna (e.g., Dyer, 1997; Townend et al., 2012; Savenije, 2012). The estuarine morphology is shaped by natural forcing such as river flow, tides, waves and human activities such as land reclamation, navigational training, sand mining and dam construction. Particularly in the last two centuries, anthropogenic impact has increased and has, in many cases, overwhelmed the influences of natural developments, causing many estuaries and deltas to be in a state of rapid transition (Wang et al., 2015; Hoitink et al., 2017). From the perspective of sustainable coastal management, it is of major significances to understand and predict the morphodynamic behavior of estuaries in response to changing natural

conditions and human activities.

In estuarine environments, the seaward decreasing river flow impact is coupled with the landward decreasing impact of tidal motion. There exists a certain place where seaward sediment transport by river offsets landward sediment transport by tides (Dalrymple and Choi, 2007; Choi et al., 2020). This inevitably results in the development of sediment bodies, like distributary mouth bars, river-channel bars and tidal ridges. They build up the skeleton of estuaries and play a major role in the hydrodynamics and sediment transport (Zhang X et al., 2020).

Morphodynamic models provide a powerful tool to investigate the formation and underlying physical mechanisms of observed morphological patterns in the real world. Geleynse et al. (2011); Leonardi et al., 2013; Xie et al. (2017a); Hoitink et al. (2017) and Luan et al. (2018) are examples of recent research efforts to address mouth bar formation, and its morphodynamic response to riverine sediment supply. Van der Wegen and Roelvink (2012), Dam et al. (2016) and Nnafie et al. (2018, 2019) addressed the importance of the estuarine planform and historic land reclamation works on the evolution of the channel-shoal patterns. However, the morphodynamics of an extended inside bar, a first order morphological feature located in the inner estuary, remains relatively unexplored, especially considering their response to human activities such as land reclamations.

The Qiantang Estuary is one of the largest macro-tidal estuaries worldwide (Fig. 1). A large longitudinal bar is developed in the inner estuary. It is the largest estuarine sediment deposit in China. With a length of around 130 km, and the highest part about 10 m above the estuary's bed, its spatial scale is at least one order larger than single or complex sandbars observed in many other

64 estuaries. The formation of this bar is due to the ample sediment supply from the adjacent
65 Changjiang (Yangtze) Estuary, of which the fluvial sediment load used to be 450 million tons per
66 year, and is transported along shore and into the Qiantang Estuary (Milliman et al., 1985; Chen et
67 al., 1990; Zhang et al., 2014, 2015). In recent years, several morphodynamic models have been
68 employed to reproduce the formation of the large bar and explore the underlying physical
69 mechanisms (Yu et al., 2012; Xie et al., 2017b; Hu et al., 2018). Based on a long series of
70 bathymetric data in the estuary, Xie et al. (2018) suggested that under natural conditions, the
71 morphodynamics of the Qiantang Estuary is controlled by a combination of river flow and tides,
72 especially by river flood events and tidal bores.

73 Since the 1960s, a large-scale coastal embankment project (LCEP) narrowing the Qiantang
74 Estuary has been gradually implemented (Fig. 1). The planform of the estuary has been changed
75 considerably. Several studies have focused on the influences of the LCEP on the hydrographical
76 regime, using water level records or numerical modeling based on shoreline changes (Zou and
77 Shen, 2017; Jin et al., 2020). But still there exist a gap between the hydrographic change and
78 morphological evolutions. Recent analysis of the bathymetrical data revealed that the bar has
79 shown a seaward movement in the last decades (Fig. 2). This raises scientific questions on the
80 underlying physical processes for the bar movement and to what extent the estuarine planform can
81 determine the dimensions of the bar within the estuary?

82 The large bar of the Qiantang Estuary is also the region where one of the most spectacular
83 and fascinating tidal bore in the world occurs, a particular hydraulic phenomenon readily observed
84 as a near-vertical wall of water traveling upriver during flood tide (Bartsch-Winkler and Lynch,

1988; Chanson, 2012). It has been long recognized that the large bar is one of the prerequisites for the bore formation (Chen et al., 1964; Chen et al., 1990; Han et al., 2003). The drastic landward rising bed level in the bar reach reduces the water depth and promotes the tidal wave deformation and eventually breaking. In recent years, several studies have focused on the turbulence properties and associated sediment transport of tidal bore based on short-term (e.g., a spring-neap tidal cycle) field observations and numerical models (e.g., Pan and Huang, 2010; Fan et al., 2014; Tu et al., 2021). However, few focused on the impact of anthropogenic morphological changes on the bore propagation.

In this contribution, we aim to explore the influence of estuarine planform on the morphological development of an inside bar, taking the large bar in the Qiantang Estuary as an example. Specific objectives are: (1) to reproduce the morphological response of the inside bar in the Qiantang Estuary to the large-scale coastal embankment works and analyze the underlying physical mechanisms; (2) to determine the controls of the bar dimensions and location and to develop a comprehensive framework of the bar morphodynamics; (3) to explore the influence of the bar evolution on the tidal bore characteristics. The Qiantang Estuary is surrounded by one of the most developed regions in China. Due to its large extent, the morphodynamic evolution of the inside bar affects the entire environment of the estuary. Therefore, studying the morphodynamic evolution of the large bar in the Qiantang Estuary not only improves our understanding of the morphodynamic behavior of the inside bar but also helps the coastal development and marine spatial planning of local government.

2. Study area

106 The Qiantang Estuary is a macro-tidal convergent estuary, located immediately south of the
107 Changjiang (Yangtze) Estuary (Fig.1). The length is 282 km and the width narrows from 98.5 km
108 at the mouth to less than 1 km at the landward end. The estuary can be divided into three reaches
109 (Han et al., 2003). The riverine reach, extending over 87 km upstream Zhakou to the Fuchun Power
110 Station, is dominated by river discharge while the effects of tides are limited. It is mainly composed
111 of coarse sand and gravel and the bed is relatively stable. The seaward reach downstream Ganpu,
112 also well known as the Hangzhou Bay, is 87 km long and controlled by tidal currents. With the
113 sediment input from the Changjiang Estuary, the Hangzhou Bay has continuously experienced net
114 deposition, with an average accumulation rate of 1.15 cm over the recent 100 years (Dai et al.,
115 2014). The estuarine reach between Zhakou and Ganpu, with a length of 108 km, is floored by
116 easily erodible, well-sorted silt and clay floored on the bed. It is controlled by the combination of
117 river flow and tidal currents. The morphological evolution in this reach is comparatively dynamic.
118 The most remarkable morphological feature of the estuary is the large longitudinal bar (Figs.
119 1b and 2). It starts from Zhapu at the middle Hangzhou Bay and elongates by about 130 km
120 landward. The bed level rises gradually from about -10 m at Zhapu to 1 m at the Qibao - Cangqian
121 reach, and then gradually decreases to be about -20 m (with respect to the Chinese National Vertical
122 Datum of 1985, the same below). There are several bends upstream of Ganpu. The thalweg and
123 tidal flats are developed at the concave and the convex banks, respectively (Fig. 1b). Between
124 Zhapu and Jinshan, a large tidal channel and a tidal flat have developed in the northern and
125 southern Hangzhou Bay, respectively (Han et al., 2003; Xie et al., 2009, 2017b). Downstream from
126 Jinshan, there is a large subaqueous plain with an average depth of about 11 m.

The annual discharge from the Qiantang River is 952 m^3/s, much smaller than the tidal prism at the mouth that can be 30×10^9 m^3 (tidal flow discharge in the order of 10^6 m^3/s) during spring tides (Xie et al., 2017a). Due to the monsoon climate, river discharge is characterized by seasonal and interannual variations. The period between April and July is the wet season, with an average peak value of 1893 m^3/s in June while the period between August and next March is the dry season, with a monthly discharge varying between 438 and 592 m^3/s (Xie et al., 2017b). Over the years, the annually averaged discharge fluctuates between 319 and 1390 m^3/s. During high flow season, the flood peaks can be more than 10,000 m^3/s, with the daily maximum being 12,787 m^3/s since the 1960s (Han et al., 2003). The Qiantang Estuary is strongly influenced by the river flood events and the tidal bore in the estuary, one of the largest in the world (Bartsch-Winkler and Lynch, 1988; Pan and Huang, 2010). As a result, the estuary is characterized by active morphological changes on seasonal and interannual time scales. Especially in the inner estuary the local bed level change can be more than 5 m in several months (Chien et al., 1964; Han et al., 2003; Xie et al., 2018) .

The tides in the estuary originate from the East China Sea and are mainly composed of a semidiurnal M_2 constituent. The mean tidal range is about 3.2 m at the mouth (Xie et al., 2017a). Landward width convergence and shallower bathymetry considerably deform the tidal waves upstream evolving into the world famous Qiantang bore. The tidal range increases landward and reaches its maximum at Ganpu, with a multi-year average of 6.0 m, and then decreases landward due to bed friction. Wind waves are weak in this area, with an annually averaged wave height of 0.5 m at the Tanxu station (water depth of about 10 m) in the Hangzhou Bay (Han et al., 2003).

Due to the large width to depth ratio, the main channel of the Qiantang Estuary used to

meander continuously, and the coastal protection revetments used to collapse frequently, resulting in lack of resources for development and navigation channel maintenance. Since the 1960s, a large-scale coastal embankment project has been carried out for the purpose of flood defense and land reclamation amongst others (Li and Dai, 1986; Han et al., 2003). The LCEP was implemented gradually seaward and basically finished in the 2010s (Fig. 2). The land reclamation mainly occurred at the middle and high flats. So far, more than 1000 km^2 land has been reclaimed and the planar shape of the estuary has been largely changed. For example, the width at Yanguan has decreased from about 10 km to about 2.5 km and at Ganpu from about 22 km to 18 km.

3. Model description

3.1. Model setup

The inside bar in the Qiantang Estuary is a longitudinal morphological feature, with the length much larger than the width and depth. Since the main body of the inside bar is located in the estuarine reach where the width is relatively small, the lateral variation of the morphology is less important. Therefore, a 1-D model can fulfill the controlling processes of the hydrodynamics and morphological evolution. Compared to the complex morphodynamic models that contain the state-of-the-art physical descriptions and parameterizations, an idealized model focuses on the prevailing morphological processes and favors an examination of the underlying physical mechanisms in a straightforward manner, through input reductions including simplified geometry and boundary conditions and formulations.

We construct an idealized 1-D morphodynamic model based on the Delft3D software

(Deltares, 2016), which has been widely used for hydrodynamics and morphodynamics in estuarine environments (e.g., Wang et al., 1995; Hibma et al., 2004; Van der Wegen and Roelvink, 2008; Van der Wegen and Jaffe, 2014; Guo et al., 2014; Zhou et al., 2017; Nnafie et al., 2019). Flow is calculated based on the horizontal shallow water equations. Transport of the suspended sediment is based on the advection-diffusion equation, in which the erosion and deposition fluxes between the bed and the water column are calculated by the well-known Krone-Partheniades formulation (Partheniades, 1965). Bed elevation is dynamically updated at each computational time step, based on the conservation of sediment mass and multiplied by a morphological factor of 10 to enhance bed level change.

This study focuses on the influences of changes in estuarine planform on the morphodynamic development of the large bar and associated hydrographic regime. Two basic cases are set. The model domain mimics the outlines of the Qiantang Estuary in the 1950s and the 2010s, representing the estuarine planforms before and after the LCEP, respectively (Fig. 3). The domain consists of a 280 km long basin with a constant width of 1 km for the first 90 km followed by a width expanding to 100 km at the mouth. Compared to the 1950s case, the coastline in the 2010s case is narrowed by 8 km at 140 km and 4 km at 200 km (the x-coordinate is defined from the landward end, as shown in Fig. 3a). The initial bed level decreases linearly from 0 m at the landward end to -9 m at the seaward end, indicating a preliminary longitudinal bed slope of 3.2×10^{-5}.

At the seaward boundary, the model is forced by a semidiurnal M_2 tide with a tidal amplitude of 2 m. A suspended sediment concentration (SSC) of 1.0 kg/m^3 is prescribed, close to the annual

190 average SSC at the mouth (ECCHE et al., 1992; Xie et al., 2017a). At the landward boundary,
191 episodic river flood events are neglected so that we can focus on the long-term morphologic
192 development of the large bar under human activities. A constant river discharge of 1000 m^3/s is
193 prescribed, close to the annually averaged discharge from the Qiantang River. The SSC is set to be
194 0.15 kg/m^3, denoting that the annual sediment supply from the Qiantang River is about 5×10^6 ton
195 (Chen et al., 2006). Both the two cases are run for 3 years of morphodynamic evolution in which
196 the bar system is formed. As a first approximation, we neglect the role of salinity stratification.
197
198 **3.2. Model runs for sensitivity analysis**
199 In order to obtain a more general understanding of the controls of the planform of the estuary
200 on the bar dimensions, an additional group of numerical experiments is conducted (Table 1). The
201 formulation of estuary convergence with a width reducing exponentially in landward direction has
202 been well adopted in many studies and can be expressed by the following classical relation (e.g.,
203 Friedrichs and Aubrey, 1994; Lanzoni and Seminara, 1998; Savenije, 2012):
204 $$B = B_0 \exp(-\frac{L-x}{L_b}) \quad (1)$$
205 in which B_0 is the width at the mouth, L is the estuary length and L_b is the convergence length.
206 Based on the widths along the estuary in the 1950s and 2010s (upper right panel in Fig.1a), it can
207 be found that the convergence length of the estuary has decreased from 65 km to 50 km, indicating
208 an increase of the convergence. The width at the estuary mouth is fixed at 100 km, since it is
209 determined by the geological background such as the Zhoushan archipelago. The width along the
210 estuary is decreased exponentially landward with convergence lengths of 20, 40, 60, 80, 100 km,

211 respectively. The other model inputs are kept invariant.

212 In an alluvial estuary, river discharge and the associated sediment supply may play an
213 important role, especially in the upper reach where smaller channel cross-sections and tidal prisms
214 prevail. River flows attenuate tidal currents through enhanced tidal friction, and constrain landward
215 saltwater intrusion by enlarging ebb currents (Godin, 1985; Savenije, 2012; Hoitink and Jay, 2016).
216 As a result, considerable morphological changes in estuarine environments may take place due to
217 the variations of river discharges. In terms of the Qiantang Estuary, it has been recognized that
218 during the high flow periods, the river flow erodes the bed and transports sediment seaward
219 whereas during the low flow periods, the tidal currents transport sediment landwards leading to
220 deposition in the inner estuary (Han et al., 2003; Xie et al., 2017b; Xie et al., 2018). In this study,
221 in order to explore the controls of river discharge on the bar dimensions, a series of sensitivity runs
222 are added on the basis of the two basic cases, with the river discharge varying from 250 to 2000
223 m^3/s with an interval of 250 m^3/s. These values fall in the reasonable range of the river discharges
224 of the Qiantang River, as mentioned in the previous section.

225

226 **4. Model results**

227 **4.1. Morphological evolution**

228 Figure 4 illustrates the processes of the morphological evolution of the estuary in the 1950s
229 and 2010s cases. In the model the large bar is formed in 3 years, in agreement with recent studies
230 (Xie et al., 2017b; Hu et al., 2018). In the 1950s case, the reach upstream 50 km has significantly
231 eroded. The sediment is transported seaward. The cumulative sediment transport through the 50

232 km transect over 3 years is 5.7×10^6 m^3. The reach downstream 175 km is eroded, tending to evolve
233 toward a subaqueous plain, and the sediment is transported landward. The cumulative sediment
234 transport through the 175 km transect over 3 years is 57.5×10^6 m^3. As a result, sediment of
235 63.2×10^6 m^3 is accumulated between 50 and 175 km, and a large bar is gradually developed. More
236 than 90% of the sediment accumulated in the bar region is from seaside, consistent with previous
237 studies on the sediment sources of the large bar (Chen et al., 1990; Zhang et al., 2015). The bar
238 apex is located at 103.5 km and its elevation is 1.10 m. Morphological development in the 2010s
239 case is similar. The bar apex is located at 122.4 km and its elevation is 0.54 m. The cumulative
240 sediment accumulation at the bar area is 58.0×10^6 m^3, smaller by 5.2×10^6 m^3 than that in the 1950s
241 case. Compared to the 1950s case, the bar apex in the 2010s case has moved seaward by 16 km
242 and lowered by 0.86 m. The landward slope of the bar (upstream the apex) is eroded by 1.5 m on
243 average whereas the seaward slope (downstream the apex) is accumulated by 1.0 m on average.

244 Overall, the simulated longitudinal profiles after 3 years are comparable with the real
245 situations (Fig. 3), indicating that the model can skillfully reproduce the morphological response
246 of the bar to the LCEP. Furthermore, the longitudinal length of the bar has decreased from 137.3
247 km to 128.8 km. This is mainly related to the seaward movement of the landward slope of the bar,
248 because the location of tail of the bar has hardly changed.

249 Similar to the 2-D morphodynamic modeling of Xie et al. (2017b), a longer than 3 year
250 simulation shows that the bar grows continuously to an unrealistic height ($\gg$10 m). In reality, the
251 growth will be constrained by erosion during high river discharge periods, i.e. river flood events.
252 In the Qiantang Estuary, flood events occur almost in each year (Han et al., 2003). Flood events

253 erode seriously the bed in the inner estuary and export sediment seaward. Over a long enough time
254 span, the sediment input by tides can be balanced by sediment export by flood events (Xie et al.,
255 2017b; Xie et al., 2018).
256
257 **4.2. Hydrodynamic and sediment transport changes**
258 The hydrodynamics and associated sediment transport are responsible for the morphological
259 dynamics in estuaries. Exploring the origin of the large bar in the Qiantang Estuary (Yu et al., 2012;
260 Xie et al., 2017b; Hu et al., 2018) suggested that landward sediment transport by flood dominance
261 is the main cause for the bar formation. Here we focus on the change of the hydrodynamic regime
262 induced by the change of the estuarine planform.
263 In the initial state, both the high and low water levels increase landward due to backwater
264 effects (e.g., Savenije, 2012; Hoitink and Jay, 2016) (Fig. 5a). The tidal range maintains around 4
265 m downstream of 90 km and decreases gradually landward due to the bed friction. The tidal bore
266 is also reproduced (Fig. 5b). After the coastal embankment, the high water level increases upstream
267 150 km due to the enhanced reflection of the tidal wave. The maximum increase is about 0.5 m.
268 The low water level increases upstream 100 km but decreases between 100 and 220 km.
269 Subsequently, the tidal range upstream 200 km is increased, with the maximum being 0.6 m.
270 Both flood and ebb velocities increase between 50 and 250 km, because the narrowing of the
271 estuary converge the tidal energy. The maximum increase of the velocities appears at around 100
272 km (Fig. 5c). Between 50 and 250 km, the flood maximum (u_f) is larger than ebb maximum (u_e),
273 with a maximum ratio of u_f/u_e of 1.74, indicating the flood dominance (Fig. 5d). Downstream 50

km and upstream 250 km, the flood maximum is less than ebb maximum, indicating the ebb dominance. After the coastal embankment, the flood dominance decreases upstream 90 km and increases downstream 90 km. Overall, the changes of the flood and ebb velocities induced by the embankment works are qualitatively consistent with the results of Zou and Shen (2017) who simulated the influences of the LCEP on the hydrodynamics in the estuary using real coastline and bathymetry.

The tidal prism Q_t, the ratio R between the river discharge and the tidal prism along the estuary are calculated as follows:

$$Q_t = \int_{t_0}^{t_0+T_f} UHBdt \tag{2}$$

$$R = \frac{\int_{t_0}^{t_0+T_f} qdt}{Q_t} \tag{3}$$

where U is the depth-averaged current velocity (m/s), H is the water depth (m), B is the width (m), t_0 is the begin of flood period, T_f is the flood duration (s), q is river discharge (m^3/s). The sediment fluxes of flood and ebb tides are function of the tidal prism, SSC and river discharge.

The tidal prism at the estuary mouth is about 28×10^9 m^3 and decreases gradually landward (Fig. 5e), in agreement with the field observation (Xie et al., 2017a). Correspondingly, the ratio R decreases from 0.18 at the landward end to less than 0.001 at the seaward end. After the embankment, the tidal prism decreased by about 30%. Hence the ratio R is increased accordingly (Fig. 5f). Sediment flux at the mouth is about 2.2×10^6 m^3 and increases slightly landward but then decreases (Fig. 5g). The net sediment flux is in the order of 10^4 m^3 per tidal cycle, being negative between 90 and 200 km, and positive upstream 90 km and downstream 250 km (Fig. 5h). Since

294 the bed level change is related to the spatial gradient of sediment transport rate, sediment will
295 accumulate in the bar area. After the embankment, the changes of sediment fluxes are similar to
296 those of tidal prisms. The sediment flux downstream 150 km decreases by about 20%. The net
297 sediment transport decreases between 100 and 170 km whereas increases between 170 and 250
298 km.

299 In the region of bar formation, both the high and low water levels upstream 100 km is lowered
300 due to the bed erosion in the upper reach (compare Fig.5a and Fig. 6a). The longitudinal water
301 level slope is decreased accordingly. The difference between the high levels in the two cases is
302 comparable with that at the initial stage, indicating that the influence of the bathymetrical change
303 is limited and the change of the high level is mainly related to the embankment. The low water
304 level in the 2010s case is about 0.1 m lower than in the 1950s case, consistent with the recent
305 finding based on field data by Jin et al. (2020) who found that the annual low levels at Zhakou,
306 Qibao and Yanguan stations have shown decreasing trends since 1960s, with the magnitude
307 between 0.05 and 0.2 m. This is because the low level in the upper reach is mainly related to the
308 local bel levels (Han et al., 2003). The bed erosion of the upper reach in the 2010s case is more
309 apparent that in the 1950s case (Fig. 4). The low level in the bar region is apparently influenced
310 by the bathymetry, and a fast lowering of the low level occurs from 100 km to 160 km. The low
311 level between 100 and 160 km is 0.1-0.4 m higher in the 2010s case than in the 1950s case, due to
312 the accumulation in the downstream slope of the large bar. As a result, the tidal range in the inner
313 estuary increases by about 0.4 m (Fig. 6b) , consistent with field data (Pan and Han, 2017). Such
314 a tidal amplification is similar to the sand extraction in the Pearl Estuary, Southern China and and

channel deepening in the Ems Estuary (Zhang et al., 2010; van Maren et al., 2015; Dijkstra et al., 2019). However, the tidal amplification in the Qiantang Estuary is not directly induced by human activities but indirectly by the response of the morphodynamic system to the LCEP.

In both cases, the ebb maximum in the inner estuary decrease due to the bed erosion (Fig. 6c). Compared to the velocities in the 1950s case, both the flood and ebb maximum increase between 50 and 130 km. Subsequently, the ratio u_f/u_e increase upstream 100 km, consistent with the tidal amplification. The peak of u_f/u_e still appears in the bar area, but its location moves seaward by 18 km (Fig. 6d).

4.3. Influence of river discharge

Fig. 7 shows an example of the longitudinal profiles of the estuary in the basic cases under the variation of river discharge, and the corresponding bed level changes under the low (500 m^3/s) and high (1500 m^3/s) discharges, compared with that under the intermediate flow (1000 m^3/s). In the low flow cases, sediment accumulation and erosion occur in the upper and lower parts of the bar, respectively, and subsequently the bar moves landwards. Vice versa in the high flow cases. The magnitudes of bed level change in the high flow case is smaller than in the low flow case, implying the bed level change is more sensitive to the river discharge variation in the low flow period.

Compared to the 1950s case, the region with significant bed level changes in the 2010s case moves seaward by about 10 km. For example, in the 1950s case, the transitional point between erosion and accumulation is located at 124 km and 132 km under the discharge of 500 m^3/s and

1500 m^3/s, respectively; whereas in the 2010s case it is at 132 km and 140 km, respectively (Fig. 7b). Chen et al. (1990); Han et al. (2003) suggested continuous water and sediment exchange between the estuary and the Hangzhou Bay. Our model results suggest that this exchange has changed as a result of the LCEP and the seaward movement of the large bar.

The location and elevation of the bar apex correlates well with the river discharge (Fig. 8). With the river discharge increasing from 250 m^3/s to 2000 m^3/s, the bar apex in the 1950s case moves seaward from 89.3 km to 109.1 km and its elevation is lowered from 2.81 m to -0.66 m. Chen et al. (1990) found similar correlations by using bathymetrical and discharge data before the beginning of the LCEP. These correlations suggest the existence of a dynamic equilibrium for the large bar, with seasonal and interannual variations depending on river discharge variations, but in balance over longer time scales. This dynamic equilibrium was also found by Fan et al. (2016) based on time-series of satellite images of the seasonal and multi-year variations of channel morphology. With the implementation of the LCEP, the correlations have been changed. On average, the location of the bar apex in the 1950s and 2010s cases is at 101.4 km and 117.0 km, respectively, and the elevation of the bar apex is 0.80 m and 0.49 m, respectively.

4.4. Influence of estuary convergence

Tidal prism depends on the estuarine planform to a large extent. One of the most important consequences of land reclamation is the reduction of tidal prism (e.g., Friedrichs and Aubrey, 1994; Lanzoni and Seminara, 1998; Todeschini et al., 2008; Pye and Blott, 2014; Wang et al., 2015). Fig. 9a shows that the tidal prism at the estuary mouth correlates with the convergence length of the

357 estuary. With the L_b decreasing from 100 km to 20 km, the prism decreases from 27.4×10^9 m^3 to
358 12.1×10^9 m^3. Accordingly, the ratio R increases (Fig. 9b). The maximum ratio for the cases of 20,
359 40, 60, 80 and 100 km are 2.8, 1.87, 1.40, 0.81 and 0.51, respectively. The ratio shows a rapid
360 reduction seaward in the upper reach (0 - 50 km) and then a relatively gentle reduction in the lower
361 reach.

362 Fig. 10 illustrates the bathymetries of the estuary under various convergence lengths. In all
363 cases, the large bar evolves. With a decreasing convergence length, the bar moves seaward and
364 becomes lower, consistent with the basic cases (Fig. 4). The apex location moves from 191.8 km
365 to 60.4 km, and elevation of the apex decreases from 3.2 m to -6.7 m, if the convergence length
366 decreases from 100 km to 20 km. Moreover, the bar length decreases from 117.2 km to 4.6 km.
367 Clear power or logarithmic relationships exist between the bar location as well as dimensions
368 (elevation of the bar apex and the bar length) and the convergence length (Fig.11).

369 The formation of a tidal bore is related to the tidal range at the mouth, the funnel shape of the
370 estuary which constraints the incoming tide and converges the tidal energy, and the subaqueous
371 bathymetry which promotes the deformation of tidal wave (Lin, 2008; Dolgopolova, 2013;
372 Bonneton et al., 2015). The strength of the tidal bore can be quantified using the relative Froude
373 number F_r (Peregrine, 1966; Chanson, 2011):

374 $$F_r = \frac{c-u_1}{\sqrt{gh_1}} \tag{4}$$

375 where c is the propagation speed of the bore, u_1 and h_1 are the current velocity and water depth
376 prior to the arrival of the bore, respectively, and g is the gravitational acceleration. For F_r >1.5~1.7

the bore is breaking, while for 1.3< F_r <1.5~1.7 the bore is undular with limited breaking. By incorporating the analytical formula for the propagation speed of a bore (Pan et al., 2008) and formula (4), Zhang S et al. (2020) suggested the relative F_r can be calculated based on the local tidal range Δh and the current velocity prior to the bore h_u:

$$F_r = \sqrt{\frac{1}{2}\left(\frac{\Delta h}{h_u}+1.5\right)^2 - \frac{1}{8}} \quad (4)$$

Fig. 12 shows the relative Froude number along the estuary after the bar formation in the cases of varying convergence length. Overall, the reach where F_r is larger than 1.7 is consistent with the morphological bulge of the bar, suggesting the importance of the bar on the tidal bore development. Similar to the development of the bar in the cases of various convergence lengths, the "bore reach" also shows a seaward movement. This is consistent with the observations and would be discussed below. Furthermore, the peak of F_r decreases with the decrease of the convergence length. The peak is 2.18, 2.17, 2.03, 1.75 and 1.41, respectively for the 5 convergence cases in order. This indicates that the tidal bore tends to be weakened with a narrowing of the estuary. A breaking bore would disappear while only an undular bore is formed if L_b is less than 20 km.

5. Discussion

5.1. What determines the inside bar location and dimensions?

Estuarine morphology results from an intricate balance between fluvial and marine processes (Dyer, 1997; Dalrymple and Choi, 2007). The relative strength of tidal prism and river discharge is often used to be a metric for the first-order estimate of estuarine morphology. For example,

downstream channel widening can be quantified by the ratio of the tidal and fluvial discharges (Nienhuis et al., 2018). Using a morphodynamic model of an idealized short estuary, Bolla Pittaluga et al. (2015) showed that the estuarine channel-bed slope tends to increase with decreasing fluvial discharge. The physical mechanism for the formation of the large inside bar in the Qiantang Estuary is also related to the ratio between the river flow and tidal prism. The planform of an estuary is one of the most important parameters controlling hydrodynamic and morphodynamic processes. Channel convergence causes a distortion of the tidal wave, strongly affects the hydrodynamics and forces the sediments to move towards the inner part of the estuary (e.g., Friedrichs and Aubrey, 1994; Lanzoni and Seminara, 1998; Todeschini et al., 2008; Savenije, 2012). Given the fact that the river discharge is invariable in the last decades, the river flow - tidal prism ratio R depends on the variation of the tidal prism. Especially the decrease of the convergence length induces a reduction of tidal prism at the estuary mouth and subsequently an increase of the ratio R (Fig. 5e and Fig. 10a). Hence the role of river discharge in the inner estuary is relatively increased, which can push the large bar seaward. Furthermore, sensitivity analysis by numerical experiments show that not only the bar location but also the bar elevation and bar length correlates well with the estuary convergence. On the other hand, when the planform of the estuary is fixed, the bar dimensions are influenced largely by the variations of the river discharge. The role of river discharge turns out to be more apparent in the case of stronger convergence of the estuary (Fig. 6 and 7).

Tidal asymmetry is an important indicator for the sediment transport and morphological pattern development (Wang et al., 2002; Van der Wegen and Roelvink, 2008; Guo et al., 2014;

418 Zhou et al., 2018). The middle reach of the estuary is characterized by flood dominance (Fig. 5d).
419 With the narrowing of the estuary, such reach is moved seaward slightly, and the area of sediment
420 accumulation moves seaward (Fig. 5h).

421 Model results in this study show that the seaward movement of the bar induced by the LCEP
422 has led to significant accumulation of the seaward slope of the bar (Fig. 4). Actually the accelerated
423 accumulation rate can extend to the inner Hangzhou Bay. Based on historical bathymetries in the
424 Hangzhou Bay, Xie et al. (2017c) found the accumulation rate in the inner Hangzhou Bay (between
425 Jinshan and Ganpu) has been apparently increased from 2.4 cm/a during the period of 1959 - 2003
426 to 13.4 cm/a during the period of 2010 - 2014. The inner Hangzhou Bay can be seen as the tail of
427 the large bar (Fig. 2). Hence the model results explain the physical mechanism of morphological
428 development since the 1960s in the Qiantang Estuary as well as the inner Hangzhou Bay.

429 Besides the estuarine planform, sediment supply is another potential factor for the
430 morphological development. The Qiantang Estuary is one of the sinks of the Changjiang River
431 sediment (Milliman et al., 1985; Chen et al., 1990; Zhang et al., 2014, 2015). In recent years,
432 sediment load of the Changjiang River has been decreasing sharply from more than 4.5×10^8 t/a
433 to less than 1.5×10^8 t/a due to soil conservation and dam constructions in the Changjiang River
434 basin, especially since the impoundment of the Three Gorges Dam in 2003 (Gao and Wang, 2008;
435 Yang et al., 2011; Milliman and Famsworth, 2011; Dai et al., 2016). As a result, the Changjiang
436 Estuary has shifted from a sediment sink to a sediment source (Yang et al., 2011; Dai et al., 2018;
437 Mei et al., 2018; Dai et al., 2021). Hydrological surveys by Xie et al. (2017a) revealed that the
438 annually-averaged net sediment flux into the Hangzhou Bay mouth has decreased slightly by about
439 10% after 2003. The slight decrease sediment supply at the bay mouth caused the erosion in the
440 outer bay in recent years (Dai et al., 2014; Xie et al., 2017c). However, its influence on the inner

441 bay and the Qiantang Estuary has been overwhelmed by the large-scale embankment project,
442 because the erosion of the outer bay provides a sediment source for the inner bay (Xie et al., 2017c).
443 It can be concluded that the morphological adjustment of the large sand bar in the Qiantang Estuary
444 in the last decades is mainly related to the LRNP.
445
446 **5.2. The rapid response of the bar to the estuary narrowing**
447 Coastal embankment works can be carried out in a relatively short period, whereas the
448 morphological response of the estuary is relatively slow (Wang et al., 2015). In most estuaries the
449 timescale for the morphology to adapt to the new hydrodynamic conditions is usually in the order
450 of decades to centuries (Van der Wegen and Roelvink, 2012; Nnafie et al., 2018). The narrowing
451 project of the Qiantang Estuary started in the earlier 1960s and basically finished in the 2010s. The
452 project was implemented gradually seaward by several stages as shown in Fig. 1a. The morphology
453 of the estuary has been changed sequentially (Pan and Han, 2017). For a long-term
454 morphodynamic modeling the initial bathymetry and the specific process of the narrowing may
455 influence the formed morphological patterns to a certain extent (Van der Wegen and Roelvink,
456 2008; Zhou et al., 2017; Nnafie et al., 2019). In this study, we excluded the actual process of the
457 project implementation by using simplified planforms and the same initial bathymetry before and
458 after the LCEP, in order to focus on the influences of estuarine planform and the first-order controls
459 of the large bar.
460 It turned out that the timescale of morphological response in the Qiantang Estuary is only
461 several years, one or two orders faster than most other estuaries (Xie et al., 2017b; Hu et al., 2018).

462 The timescale for the morphological evolution is related to the sediment transport rate (Van Rijn,
463 1993). The Qiantang Estuary is characterized by the strong tidal currents, especially influenced by
464 the tidal bore, which result in large sediment transport rate (Han et al., 2003; Pan and Huang, 2010;
465 Fan et al., 2014; Xie et al., 2018). Field observations showed that sediment flux over a flood or
466 ebb period at the Ganpu transect is in the order of 10^6 m^3 (Han et al., 2003) and during normal
467 river discharge periods the sediment accumulation in the estuarine reach can be in the order of 10^6
468 m^3 in several months (Xie et al., 2018), in agreement with the present model results.

469 To the authors' knowledge, the Sittaung Estuary, Myanmar, is the only macro-tidal estuary
470 comparable with the Qiantang Estuary in terms of the fast morphodynamic adaptation rate. The
471 length of the estuary is 220 km, and it is also funnel-shaped. Sediments are also constituted by silt
472 and clay with median grain size ranging between 0.02 and 0.04 mm (Shimozono et al., 2019; Choi
473 et al., 2020). Recently, Ahmed et al. (2019) reproduced the morphological patterns in the Sittaung
474 Estuary using a morphodynamic model. Starting from an initial bed with a constant slope, the
475 channel-shoal pattern in recent years was reproduced well with a calculation time of only several
476 months.

477

478 **5.3. The influence of the bar evolution on the tidal bore**

479 The Qiantang Estuary is characterized by one of the biggest tidal bores in the world. The bore
480 scenes attract millions of tourists each year. It is also an important cultural resource, symbolizing
481 the local people's spirit of trendsetter. Therefore, to what extent the LCEP influences the Qiantang
482 bore is one of great interests to coastal scientists, engineers and managers.

Historically, the location of the bore occurrence was further west than the present age. For example, in the Song Dynasty, about 1000 years ago, the location used to be upstream of Wenyan, about 70 km upstream of Yanguan (Chen et al., 1964). Presently the most spectacular tidal bore occurs at the Yanguan reach (Lin, 2008; Pan and Huang, 2010; Tu et al., 2021). In recent years, a breaking bore has been frequently witnessed at Shangyu, about 40 km downstream of Yanguan, indicating that the place of the bore occurrence has probably moved further seaward.

However, aside from the historical documents of the Qiantang bore, field records of the bore are very scare, making it difficult to link the bore formation with the long-term morphological evolution. Based on scale model experiment, Zeng et al. (2017) suggested that embankments near Jianshan, about 10 km long and 2.5 km wide, resulted in an increase of about 0.1 m of the bore height, due to the enhancement of the tidal wave reflection. They also suggested that if a larger embankment is carried out, the tidal prism from the East China Sea will be decreased and hence weaken the Qiantang bore. Recently, based on numerical models, Zhang S et al. (2020) and De Ridder (2017) tested the influences of the bathymetrical changes on the tidal bores in the Qiantang Estuary and the Sittuang Estuary, respectively. Increasing or reducing the bed elevation in the estuaries by a uniform value, their results showed that the bathymetry plays an important role in the bore formation and propagation. In this study, we reproduced the morphological response of the bar to the LCEP and predicted the bar location and dimensions under further narrowing in the future. It turned out that with the change of the estuarine planform and the seaward movement of the large bar, the reach for breaking bore conditions moves seaward. This explains the physical mechanisms for the historical and recent evolutions of the place of the bore occurrence. It is notable

that if the estuary is narrowed further in the future, the place of the bore occurrence would move further seaward, and would be even in danger of disappearing (Fig. 12). For the estuarine regulation in the future, attention must be paid to the influence of the morphological evolution on the tidal bore

The tidal bore is highly influenced by the bar morphology. In turn, the tidal bore also exerts great impact on the bar morphology because of the associated strong currents and sediment transport capacity. The results of the present morphodynamic model show that in addition to the seaward movement of the large bar due to the estuary narrowing, the "bore reach" also shows a seaward moving trend. It can be concluded that the morphologically active reach in the Qiantang Estuary which is strongly influenced by the bore has moved seaward in the last decades.

6. Conclusions

This study focused on the controls of the inside bar location and dimensions, taking the Qiantang Estuary as an example. Using idealized model geometries mimicking the planforms of the Qiantang Estuary in the 1950s and the 2010s, the morphological response of the large bar to the large-scale coastal embankment project was reproduced first, and then sensitivity analyses of the convergence length of the estuary and the variations of river discharge were carried out.

The morphological response of the large bar to the narrowing project is only several years. The rapid response is related to the strong tidal currents and large sediment fluxes. With the large-scale narrowing project of the Qiantang Estuary, the apex of the large inside bar has moved seaward by 15 km and lowered by 0.86 m. For the first-order estimation of the morphology, the seaward

movement can be attributed to the increase of the ratio between river flow and tidal prism at the mouth. The tidal prism correlates with the estuarine planform under a similar tide. A shorter convergence length results in a decrease of tidal prism, and an increase of the ratio between river discharge and tidal prism. The bar movement is also related to the change of tidal asymmetry along the estuary and subsequently the change of net sediment transport over a tidal cycle.

The locations, length and elevations of the inside bar depend on the degree of the convergence of the estuary. The bar moves seaward, and the bar length decreases with a decrease of the convergence length. River discharge also plays important role on the bar location and dimensions. Good relationships exist between river discharge and the location and elevation of the bar apex. Such relationship would be changed with the change of the estuarine planform.

The bar evolution has significant influences on the hydrological regime. The erosion in the upper reach lowers the local low water level and amplifies the tides, whereas the accumulation in the downstream slope of the bar increases the local low water level. Particularly, with the change of the estuarine planform and the seaward movement, the place of the tidal bore occurrence shows a seaward moving and the strength of the tidal bore shows a decreasing trend, explaining the historical and recent evolution of the Qiantang bore. In turn, the morphologically active reach in the estuary strongly influenced by river discharge and the tidal bore also moves seaward.

Acknowledgments

This research was supported by the National Natural Science Foundation of China (No. 41676085) and Zhejiang Provincial Natural Science Foundation of China (No. LY16D060004).

We wish to thank two anonymous reviewers for their constructive comments which improved the paper greatly.

Data availability

The bathymetric data are available at https://zenodo.org/record/4915584#.YMC0T5yOM2z.

References

Ahmed, T.S., Egashira, S., Harada, D, and Yorozuya, A., 2019. Sediment transportation and sand bar deformation owing to tidal currents in Sittaung River Estuary, Myanmar. *Journal of Japan Scociety of Civil Engineering (Ser. B1)*, 75(2), 1027-1032, doi: 10.2208/jscejhe.75.2_I_1027.

Bartsch-Winkler, S., and Lynch, D.K., 1988. Catalog of worldwide tidal bore occurrences and characteristics. *USGS Circular*, 1022, l-17.

Bolla Pittaluga, M., Tambroni, N., Canestrelli, A., Slingerland, R., Lanzoni, S., and Seminara, G., 2015. Where river and tide meet: The morphodynamic equilibrium of alluvial estuaries. *Journal of Geophysical Research: Earth Surface*, 120, doi: 10.1002/2014JF003233.

Canestrelli, A., Lanzoni, S., and Fagherazzi, S., 2013. One-dimensional numerical modeling of the long-term morphodynamic evolution of a tidally-dominated estuary: The lower Fly River (Papua New Guinea). *Sedimentary Geology*, 301, 107-119, doi: 10.1016/j.sedgeo.2013.06.009.

Chanson, H., 2012. *Tidal Bores, Aegir, Eagre, Mascaret, Pororoca: Theory and Observations*. World Science, Singapore.

Chanson, H.B., 2011. Two-phase flow in hydraulic jumps at large Froude number. *Journal of*

Hydraulic Engineering, 137(4), 451-460, doi: 10.1061/(ASCE)HY.1943-7900.0000323.

Chen, J.Y., Liu, C.Z., Zhang, C.L., and Walker, H.J., 1990. Geomorphological development and sedimentation in Qiantang Estuary and Hangzhou Bay. *Journal of Coastal Research*, 6(3), 559-572, doi: 10.2307/4297719.

Chen, J.Y., Luo, Z.D., Chen, D.C., Xu, H.G., and Qiao, P.N., 1964. The formation and historical evolution of the sandbar in Qiantang estuary (in Chinese). *Acta Geographica Sinica*, 30(2), 109-113.

Chen, S.M., Han, Z.C., and Hu, G.J., 2006. Impact of human activities on the river reach in the Qiantang Estuary (in Chinese with English abstract). *Journal of Sediment Research*, (4), 61-67.

Chien, N., Sie, H.S., Chow, C.T., and Lee, Q.P., 1964. The fluvial processes of the big sand bar inside the Chien Tang Chiang Estuary (in Chinese with English abstract). *Acta Geographica Sinica*, 30(2), 124-142.

Choi, K., Kim, D., and Jo, J., 2020. Morphodynamic evolution of the macrotidal Sittaung River estuary, Myanmar: Tidal versus seasonal controls. *Marine Geology*, 430, 106367, doi: 10.1016/j.margeo.2020.106367.

Dai, Z.J., 2021. *Changjiang riverine and estuarine hydro-morphodynamic processes: in the context of Anthropocene era*. Springer.

Dai, Z.J., Fagherazzi, S., Mei, X., and Gao, J., 2016. Decline in suspended sediment concentration delivered by the Changjiang (Yangtze) River into the East China Sea between 1956 and 2013. *Geomorphology*, 268, 123-132, doi: 10.1016/j.geomorph.2016.06.009.

588 Dai, Z.J., Liu, J.T., Xie, H.L., and Shi, W.Y., 2014. Sedimentation in the outer Hangzhou Bay,
589 China: the influence of Changjiang sediment load. *Journal of Coastal Research*, 30, 1218-
590 1225, doi: 10.2112/jcoastres-d-12-00164.1.
591 Dai, Z.J., Mei, X., Darby, S.E., Lou, Y., and Li, W., 2018. Fluvial sediment transfer in the
592 Changjiang (Yangtze) river-estuary depositional system. *Journal of Hydrology*, 566, 719-
593 734, doi: 10.1016/j.jhydrol.2018.09.019.
594 Dalrymple, R.W., and Choi, K., 2007. Morphologic and facies trends through the fluvial–marine
595 transition in tide-dominated depositional systems: a schematic framework for environmental
596 and sequence-stratigraphic interpretation. *Earth-Science Reviews*, 81(3), 135-174, doi:
597 10.1016/j.earscirev.2006.10.002.
598 Dam, G., Van der Wegen, M., Labeur, R., and Roelvink, D., 2016. Modeling centuries of estuarine
599 morphodynamics in the Western Scheldt estuary. *Geophysical Research Letters*, 43 (8), 3839-
600 3847, doi: 10.1002/2015GL066725.
601 De Ridder, M.P., 2017. *The tidal bore in the Sittaung River - a sensitivity analysis of the*
602 *propagation*. Unpublished master thesis, The Delft University of Technology.
603 Deltares, 2016. User manual Delft3d-Flow: Simulation of multi-dimensional hydrodynamic flows
604 and transport phenomena, including sediments.
605 Dijkstra, Y.M., Schuttelaars, H.M., Schramkowski, G.P., and Brouwer, R.L., 2019. Modeling the
606 transition to high sediment concentrations as a response to channel deepening in the Ems
607 River Estuary. *Journal of Geophysical Research: Oceans*, 124, 1578-1594, doi:
608 10.1029/2018JC014367.

609 Dolgopolova, E.N., 2013. The conditions for tidal bore formation and its effect on the transport of
610 saline water at river mouths. *Water Resources*, 40(1), 16-30, doi:
611 10.1134/S0097807813010028.
612 Dyer, K.R., 1997. *Estuaries - Physical Introduction*. John Wiley and Sons, Chichester.
613 ECCHE (Editorial Committee for Chinese Harbors and Embayments), 1992. *Chinese Harbours*
614 *and Embayments* (Part V, in Chinese). China Ocean Press, Beijing.
615 Fan, D.D., Tu, J.B., Shang, S., and Cai, G.F., 2014. Characteristics of tidal-bore deposits and facies
616 associations in the Qiantang Estuary, China. *Marine Geology*, 348, 1-14, doi:
617 10.1016/j.margeo.2013.11.012.
618 Fan, D.D., Tu, J.B., Shang, S., Chen, L.L., and Zhang, Y., 2016. Morphodynamics and sedimentary
619 facies in a tidal-fluvial transition with tidal bores (the middle Qiantang Estuary, China). In:
620 Tessier, B., and Reynaud, J.Y., (eds.), Contribution to Modern and Ancient Tidal
621 Sedimentology: Proceedings of the Tidalites 2012 Conference, IAS Special Publication, 48,
622 75-92.
623 Friedrichs, C.T., and Aubrey, D.G., 1994. Tidal propagation in strongly convergent channels.
624 *Journal of Geophysical Research*, 99(C2), 3321-3336, doi: 10.1029/93JC03219.
625 Gao, S., and Wang Y.P., 2008. Material fluxes from the Changjiang River and their implications
626 on the adjoining continental shelf ecosystem. *Continental Shelf Research*, 28, 1490-1500, doi:
627 10.1016/j.csr.2007.02.010.
628 Geleynse, N., Storms, J.E.A., Walstra, D.J.R., Jagers, H.R.A., Wang, Z.B., and Stive, M.J.F.,
629 2011. Controls on river delta formation; insights from numerical modelling. *Earth and*

630 *Planetary Science Letters*, 302(1-2), 217-226, doi:10.1016/j.epsl.2010.12.013.

631 Godin, G., 1985. Modification of river tides by the discharge. *Journal of Waterway, Port, Coastal*
632 *and Ocean Engineering*, 111(2), 257-274, doi: 10.1061/(ASCE)0733-950X(1985)111:2(257).

633 Guo, L.C., Van der Wegen, M., Roelvink, J.A., and He, Q., 2014. The role of river flow and tidal
634 asymmetry on 1-D estuarine morphodynamics. *Journal of Geophysical Research: Earth*
635 *Surface*, 119, 2315-2334, doi: 10.1002/2014JF003110.

636 Han, Z.C., Dai, Z.H., and Li, G.B., 2003. *Regulation and Exploitation of Qiantang Estuary* (in
637 Chinese). China Water Power Press, Beijing.

638 Hibma, A., Stive, M.J.F, and Wang, Z.B., 2004. Esturine morphodynamics. *Coastal Engineering*,
639 51, 765-778, doi: 10.1016/j.coastaleng.2004.07.008.

640 Hoitink, A.J.F., Wang, Z.B., Vermeulen, B., Huismans, Y., and Kastner, K., 2017. Tidal controls
641 on river delta morphology. *Nature Geoscience*, 10, 637-645, doi: 10.1038/ngeo3000.

642 Hoitink, A.J.F., and Jay, D.A., 2016. Tidal river dynamics: implications for deltas. *Reviews of*
643 *Geophysics*, 54, 240-272, doi: 10.1002/2015RG000507.

644 Hu, P., Han, J.J., Li, W., Sun, Z.L., and He, Z.G., 2018. Numerical investigation of a sandbar
645 formation and evolution in a tide-dominated estuary using a hydro-sediment-morphodynamic
646 model. *Coastal Engineering Journal*, 60(4), 466-483, doi: 10.1080/21664250.2018.1529263.

647 Jin, G., Zeng, J., Tang, Z., and Hu, C., 2020. Variation trends of tidal characteristics in the Qiantang
648 River Estuary and cause analysis (in Chinese with English abstract). *Marine Science Bulletin*,
649 39(4), 456-463.

650 Lanzoni, S., and Seminara, G., 1998. On tide propagation in convergent estuaries. *Journal of*

651 *Geophysical Research*, 103(C13), 30793-30812, doi: 10.1029/1998JC900015.
652 Leonardi, N., Canestrelli, A., Sun, T., and Fagherazzi, S.E., 2013. Effect of tides on mouth bar
653 morphology and hydrodynamics. *Journal of Geophysical Research*, 118, 4169-4183, doi:
654 10.1002/jgrc.20302.
655 Li, G.B., and Dai, Z.H., 1986. Fluvial processes and reclamation of the Qiantang Estuary.
656 International Journal of Sediment Research, 1 (1), 56-66.
657 Lin, B.Y., 2008. *Characteristics of Qiantang Bore* (in Chinese). Chinese Ocean Press, Beijing.
658 Luan, H.L., Ding, P.X., Wang, Z.B., Yang, S.L., and Lu, J.Y., 2018. Morphodynamic impacts of
659 large-scale engineering projects in the Yangtze River delta. *Coastal Engineering*, 141, 1-11,
660 doi: 10.1016/j.coastaleng.2018.08.013.
661 Mei, X., Dai, Z., Wei, W., Li, W., Wang, J., and Sheng, H., 2018b. Secular bathymetric variations
662 of the North Channel in the Changjiang (Yangtze) Estuary, China, 1880-2013: causes and
663 effects. *Geomorphology*, 303, 30-40, doi: 10.1016/j.geomorph.2017.11.014.
664 Milliman, J.D., Shen, H.T., Yang, Z.S., and Robert, H.M., 1985. Transport and deposited of river
665 sediment in the Changjiang estuary and adjacent continental shelf. *Continental Shelf Research*,
666 4, 37-45, doi: 10.1016/0278-4343(85)90020-2.
667 Nienhuis, J.H., Hoitink, A.J.F., and Törnqvist, T.E., 2018. Future change to tide-influenced deltas.
668 *Geophysical Research Letters*, 45, 3499-3507, doi: 10.1029/2018GL077638.
669 Nnafie, A., Swart, H.E., De Maerschalck, B., Van Oyen, T., Van der Vegt, M., and Van der Wegen,
670 M., 2019. Closure of secondary basins causes channel deepening in estuaries with moderate
671 to high friction. *Geophysical Research Letters*, 46(22), 13209-13216, doi:

672 10.1029/2019gl084444.
673 Nnafie, A., Van Oyen, T., De Maerschalck, B., Van der Vegt, M., and Van der Wegen, M.,
674 2018. Estuarine channel evolution in response to closure of secondary basins: an
675 observational and morphodynamic modeling study of the Western Scheldt Estuary. *Journal of*
676 *Geophysical Research: Earth Surface*, 123(1), 167-186, doi: 10.1002/2017jf004364.
677 Pan, C.H., and Huang, W.R., 2010. Numerical Modeling of Suspended Sediment Transport
678 Affected by Tidal Bore in Qiantang Estuary. *Journal of Coastal Research*, 26(6), 1123-1132,
679 doi: 10.2307/40928851.
680 Pan, C.H., Lu, H.Y., and Zeng, J., 2008. Characteristic and numerical simulation of tidal bore in
681 Qiantang River (in Chinese with English abstract). *Hydro-Science and Engineering*, (2), 1-9.
682 Partheniades, E.A., 1965. Erosion and deposition of cohesive soils. *Journal of the Hydraulics*
683 *Division*, 91(HY1), 4204, doi: 10.3109/15622970109026808.
684 Peregrine, D.H., 1966. Calculations of the development of an undular bore. *Journal of Fluid*
685 *Mechanisms*, 25, 321-330, doi: 10.1017/S0022112066001678.
686 Pye, K., and Blott, S.J., 2014. The geomorphology of UK estuaries: the role of geological controls,
687 antecedent conditions and human activities. *Estuarine, Coastal and Shelf Science*, 150, 196-
688 214, doi: 10.1016/j.ecss.2014.05.014.
689 Savenije, H.H.G., 2012. *Salinity and tides in alluvial estuaries* (Second Completely Revised
690 Edition). https://salinityandtides.com/
691 Shimozono, T., Tajima, Y., Akamatsu, S., Matsuba, Y., and Kawasaki, A., 2019. Large-scale
692 channel migration in the Sittang River Estuary. *Scientific Reports*, 9, 9862, doi: 10.1007/978-

981-15-0291-0_163.

Todeschini, I., Toffolon, M., and Tubino, M., 2008. Long-term morphological evolution of funnel-shape tide-dominated estuaries. *Journal of Geophysical Research*, 113, C05005, doi: 10.1029/2007JC004094.

Townend, I., 2012. The estimation of estuary dimensions using a simplified form model and the exogenous controls. *Earth Surface Processes and Landforms*, 37(15), 1573-1583, doi: 10.1002/esp.3256.

Tu, J.B., Fan, D.D., and Voulgaris, G., 2021. Field observations of turbulence, sediment suspension, and transport under breaking tidal bores. *Marine Geology*, 437(3), 106498, doi: 10.1016/j.margeo.2021.106498.

Van der Wegen, M., and Jaffe, B.E., 2014. Processes governing decadal-scale depositional narrowing of the major tidal channel in San Pablo Bay, California, USA. *Journal of Geophysical Research: Earth Surface*, 119, doi: 10.1002/2013JF002824.

Van der Wegen, M., and Roelvink, J., 2008. Long-term morphodynamic evolution of a tidal embayment using a two-dimensional, process-based model. *Journal of Geophysical Research: Oceans*, 113 (C3), doi: 10.1029/2006JC003983.

Van der Wegen, M., and Roelvink, J.A., 2012. Reproduction of estuarine bathymetry by means of a process-based model: Western Scheldt case study, the Netherlands. *Geomorphology*, 179, 152-167, doi: 10.1016/j.geomorph.2012.08.007.

Van Maren, D.S., Winterwerp, J.C., and Vroom, J., 2015. Fine sediment transport into the hyper-turbid lower Ems River: The role of channel deepening and sediment-induced drag reduction.

714 *Ocean Dynamics*, 65(4), 589-605, doi: 10.1007/s10236-015-0821-2
715 Van Rijn, L.C. (1993), *Principles of sediment transport in rivers, estuaries and coastal seas*, Aqua
716 Publication, Amsterdam.
717 Wang, Z.B., Jeuken, M., Gerritsen, H., De Vriend, H.J., and Kornman, B., 2002. Morphology and
718 asymmetry of the vertical tide in the Westerschelde estuary. Continental Shelf Research, 22
719 (17), 2599-2609, doi: 10.1016/S0278-4343(02)00134-6.
720 Wang, Z.B., Louters, T., and De Vriend, H.J., 1995. Morphodynamic modelling of a tidal inlet in
721 the Wadden Sea. *Marine Geology*, 126, 289-300, doi: 10.1016/S0278-4343(02)-00134-6.
722 Wang, Z.B., Van Maren, D.S., Ding, P.X., Yang, S.L., Van Prooijen, B.C., de Vet, P.L.M.,
723 Winterwerp, J.C., De Vriend, H.J., Stive, M.J.F., and He, Q., 2015. Human impacts on
724 morphodynamic thresholds in estuarine systems. *Continental Shelf Research*, 111, 174-183,
725 doi: 10.1016/j.csr.2015.08.009.
726 Xie, D.F, Gao, S., Wang, Z.B., Pan, C.H, Wu, X., and Wang, Q., 2017b. Morphodynamic modeling
727 of a large inside sandbar and its dextral morphology in a convergent estuary: Qiantang Estuary,
728 China. *Journal of Geophysical Research: Earth Surface*, 122(8), 1553-1572, doi:
729 10.1002/2017JF004293.
730 Xie, D.F., Pan, C.H., Wu, X., Gao, S., and Wang, Z.B., 2017c. Local human activities overwhelm
731 decreased sediment supply from the Changjiang River: Continued rapid accumulation in the
732 Hangzhou Bay-Qiantang Estuary system. *Marine Geology*, 392, 66-77, doi:
733 10.1016/j.margeo.2017.08.013.
734 Xie, D.F., Pan, C.H., Gao, S., and Wang, Z.B., 2018. Morphodynamics of the Qiantang Estuary,

China: Controls of river flood events and tidal bores. *Marine Geology*, 406, 27-33, doi: 10.1016/j.margeo.2018.09.003.

Xie, D.F., Pan, C.H., Wu, X., Gao, S., and Wang, Z.B., 2017a. The variations of sediment transport patterns in the outer Changjiang Estuary and Hangzhou Bay over the last 30 years. *Journal of Geophysical Research: Oceans*, 122, 2999-3020, doi: 10.1002/2016JC012264.

Xie, D.F., Wang, Z.B., Gao, S., and de Vriend, H.J., 2009. Modeling the tidal channel morphodynamics in a macro-tidal embayment, Hangzhou Bay, China. *Continental Shelf Research*, 29, 1757-1767, doi: 10.1016/j.csr.2009.03.009.

Yang, S.L., Milliman, J.D., Li P., and Xu K.H., 2011. 50,000 dams later: Erosion of the Yangtze River and its delta. *Global and Planetary Change*, 75, 14-20, doi: 10.1016/j.gloplacha.2010.09.006.

Yu, Q., Wang, Y.W., Gao, S., and Flemming, B., 2012. Modeling the formation of a sand bar within a large funnel-shaped, tide-dominated estuary: Qiantangjiang Estuary, China. *Marine Geology*, 299-302, 63-76, doi:10.1016/j.margeo.2011.12.008.

Zeng, J., Chen, G., Pan, C.H., and Zhang, Z.Y., 2017. Effect of dike line adjustment on the tidal bore in the Qiantang Estuary, China. *Journal of Hydrodynamics*, 29(3), 452-459, doi: 10.1016/S1001-6058(16)60756-4.

Zhang, S., Pan, C.H., and Cheng, W.L., 2020. Effect of dike line adjustment on the tidal bore in the Qiantang Estuary, China (in Chinese with English abstract). *The Coastal Engineering*, 38(1), 130-139.

Zhang, W., Ruan, X., Zheng, J., Zhu, Y., and Wu, H., 2010. Long-term change in tidal dynamics

and its cause in the Pearl River Delta, China. *Geomorphology*, 120 (3-4), 209-223, doi: 10.1016/j.geomorph.2010.03.031.

Zhang, X., Dalrymple, R.W., Yang, S.Y., Lin, C.M., and Wang, P., 2015. Provenance of Holocene sediments in the outer part of the Paleo-Qiantang River estuary, China. *Marine Geology*, 366, 1-15, doi: 10.1016/j.margeo.2015.04.008.Zhang, X., Lin, C.M., Dalrymple, R.W., Gao, S., and Li, Y.L., 2014. Facies architecture and depositional model of a macrotidal incised-valley succession (Qiantang River estuary, eastern China), and differences from other macrotidal systems. *Geological Society of America Bulletin*, 126 (3-4), 499-522, doi: 10.1130/B30835.1.

Zhang, X.D., Fan, D., Yang, Z., Xu, S., Chi, W., and Wang, H., 2020. Sustained growth of river-mouth bars in the vulnerable Changjiang Delta. *Journal of Hydrology*, 590, 125450, doi: 10.1016/j.jhydrol.2020.125450.

Zhou Z., Coco G., Townend I., et al., 2017. Is "Morphodynamic Equilibrium" an oxymoron. *Earth-Science Reviews*, 165: 257-267, doi: 10.1016/j.earscirev.2016.12.002.

Zhou Z., Coco G., Townend I., Gong Z., Wang Z.B., and Zhang C.K., 2018. On the stability relationships between tidal asymmetry and morphologies of tidal basins and estuaries. *Earth Surface Processes and Landforms*, 43(9): 1943-1959, doi: 10.1002/esp.4366.

Zou, Z.N., and Shen, Y.M., 2017. Influence of the reclamation project at Qiantang estuary on the hydrodynamics and water environment in Hangzhou bay (in Chinese with English abstracyt). *Port and Waterway Engineering*, (1), 26-33.

776 **Table and figure captions**

777 **Table 1.** Overview of model input variations in the sensitivity analysis.

778 **Fig.1.** (a) Location of the Qiantang Estuary; (b) Bathymetry of the estuarine reach measured in
779 November, 2020. The colored shades in panel (a) indicate the progress of the large-scale coastal
780 embankment project since the 1950s.

781 **Fig. 2.** The laterally averaged longitudinal bathymetries in the 1960s and the 2010s, after Pan and
782 Han (2017).

783 **Fig. 3.** Sketch of the modeled estuary. (a) Geometry (top view); (b) initial bathymetry (side view).

784 **Fig. 4.** Modeled bathymetries of the bar at the bar formation (a) and the development of the
785 longitudinal profiles of the estuary. The arrows across 50 km and 175 km denote the directions
786 of the cumulative sediment transport over 3 years.

787 **Fig. 5.** Hydrodynamics and sediment transports along the estuary at the initial states. (a) High, low
788 tidal levels and tidal ranges, (b) the water levels at four instants in the 2010s case, (c) maximum
789 flood and ebb velocities, (d) the ratio between maximum flood velocity to maximum ebb
790 velocity, (e) flood and ebb water fluxes over one tidal cycle, (f) the ratio between river flow
791 and prism, (g) cumulative sediment transport and (h) the net sediment transport over one tidal
792 cycle.

793 **Fig. 6.** Hydrodynamics along the estuary after 3 years. (a) High, low tidal levels and tidal ranges,
794 (b) the water levels at four instants in the 2010s case, (c) the maximum flood and ebb velocities,
795 and (d) the flood and ebb maximum ratio.

796 **Fig. 7.** Longitudinal profiles for various river discharges after 3 years (a) and the bed level changes

797 compared to that of 1000 m^3/s cases (b).

798 Fig. 8. Simulated correlations between the location (a) and elevation (b) of the bar apex and the
799 river discharge.

800 **Fig. 9.** Influences of the convergence length on the tidal prism at the estuary mouth (a), and the
801 river flow - prism ratio along the estuary (b).

802 **Fig. 10.** The cross-sectional averaged longitudinal profiles at the bar formation for the cases of
803 various estuary convergence.

804 **Fig. 11.** Correlations between the bar dimensions and the convergence length.

805 **Fig. 12.** Relative Froude number along the estuary after 3 years in the cases of various convergence
806 lengths.

807 **Table 1.**

Group	Estuary planform	River discharge
1	based on shoreline in the 1950s and 2010s	1000 m^3/s
2	L_b=20, 40, 60, 80, 100 km	1000 m^3/s
3	based on shoreline in the 1950s	250 - 2000 m^3/s, with an interval of 250 m^3/s
4	based on shoreline in the 2010s	250 - 2000 m^3/s, with an interval of 250 m^3/s

808

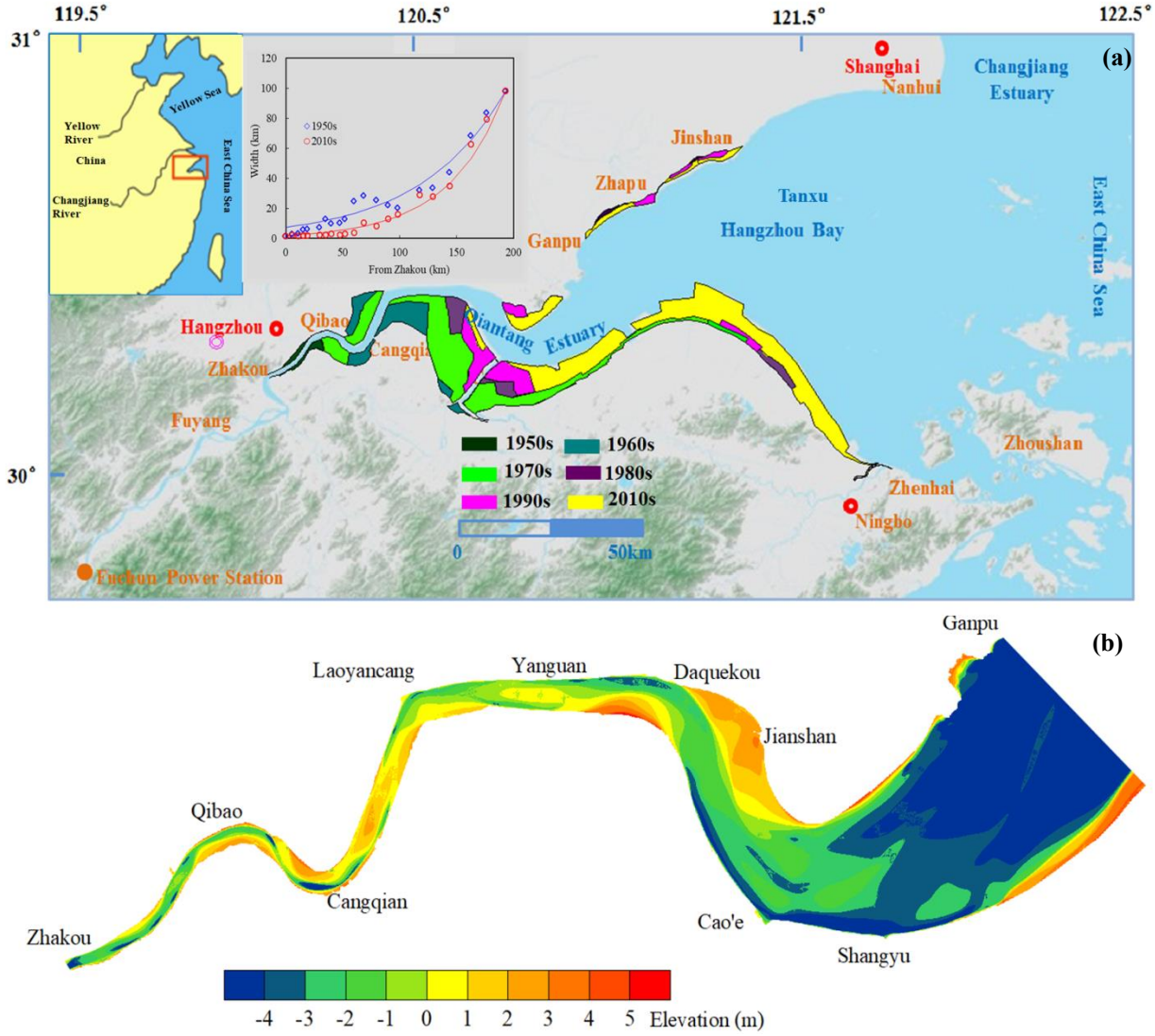
119.5°
120.5°
121.5°
122.5°
31°
30°
(a)
Yellow Sea
Yellow River
China
Changjiang River
East China Sea
1950s
2010s
Width (km)
From Zhakou (km)
Shanghai
Nanhui
Changjiang Estuary
Jinshan
Zhapu
Ganpu
Tanxu
Hangzhou Bay
East China Sea
Hangzhou
Qibao
Cangqian
Qiantang Estuary
Zhakou
Fuyang
1950s
1960s
1970s
1980s
1990s
2010s
0
50km
Zhoushan
Zhenhai
Ningbo
Fuchun Power Station
(b)
Ganpu
Laoyancang
Yanguan
Daquekou
Jianshan
Qibao
Cangqian
Zhakou
Cao'e
Shangyu
-4 -3 -2 -1 0 1 2 3 4 5 Elevation (m)

Fig.1.

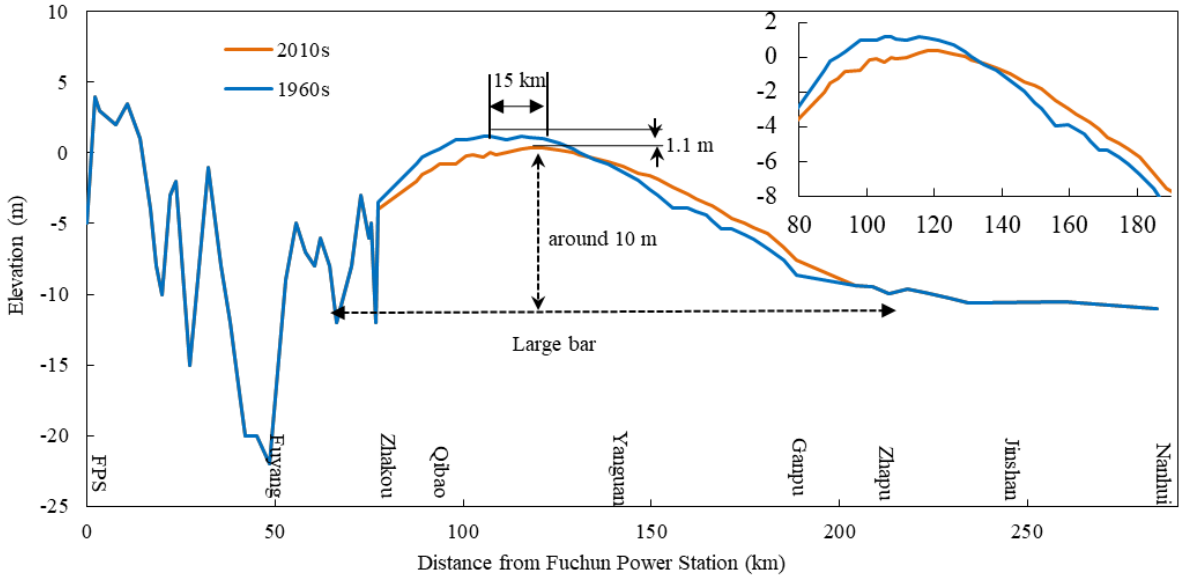
2010s
1960s
15 km
1.1 m
around 10 m
Large bar
Elevation (m)
Distance from Fuchun Power Station (km)
FPS
Fuyang
Zhakou
Qibao
Yangtuan
Ganpu
Zhapu
Jinshan
Nanhui

811

812 **Fig. 2.**

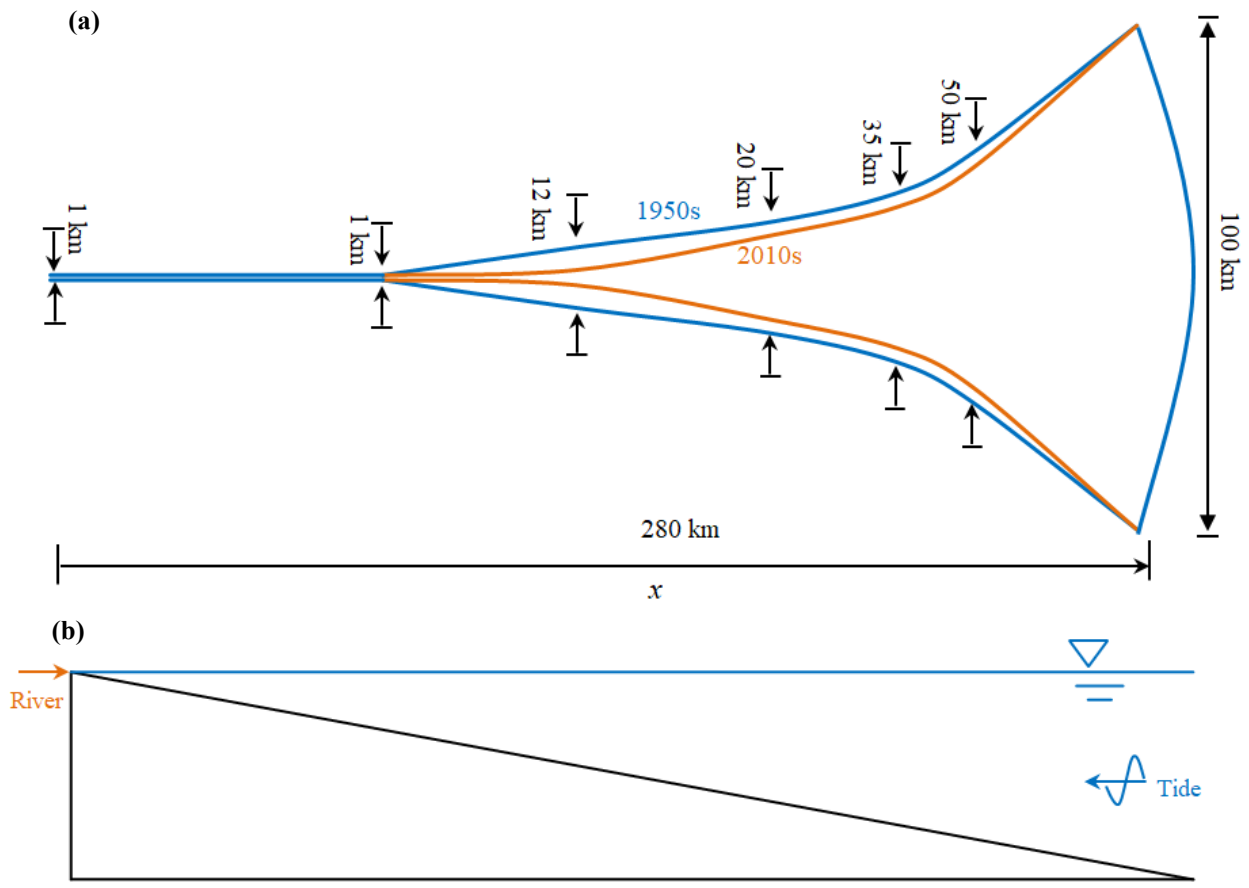
(a)
1 km
1 km
12 km
20 km
35 km
50 km
1950s
2010s
100 km
280 km
x
(b)
River
Tide

Fig. 3.

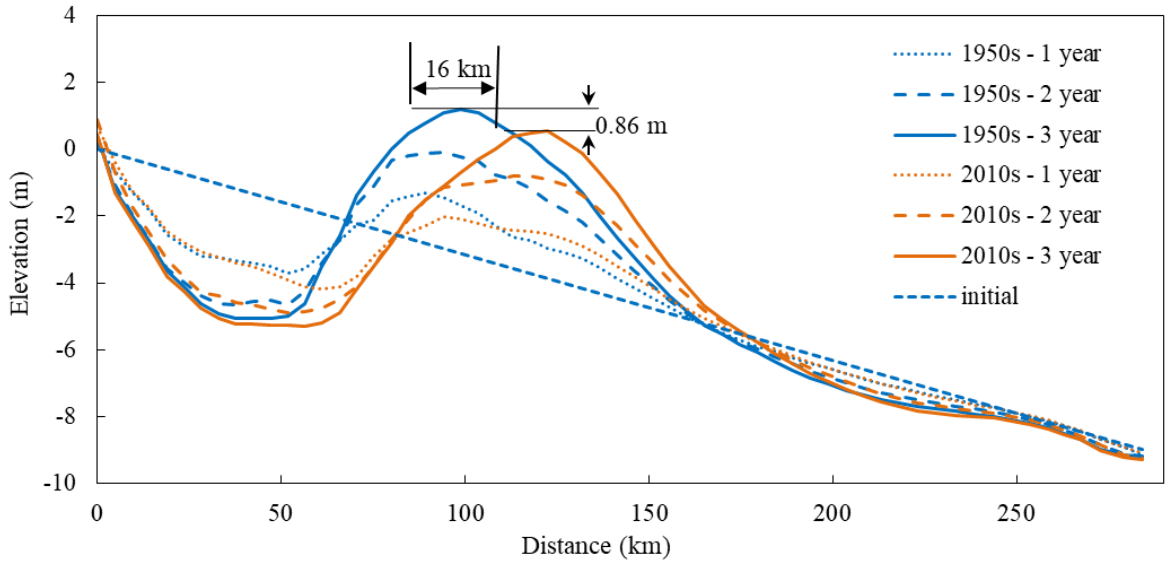
16 km
0.86 m
1950s - 1 year
1950s - 2 year
1950s - 3 year
2010s - 1 year
2010s - 2 year
2010s - 3 year
initial
Elevation (m)
Distance (km)
4
2
0
-2
-4
-6
-8
-10
0
50
100
150
200
250

Fig. 4.

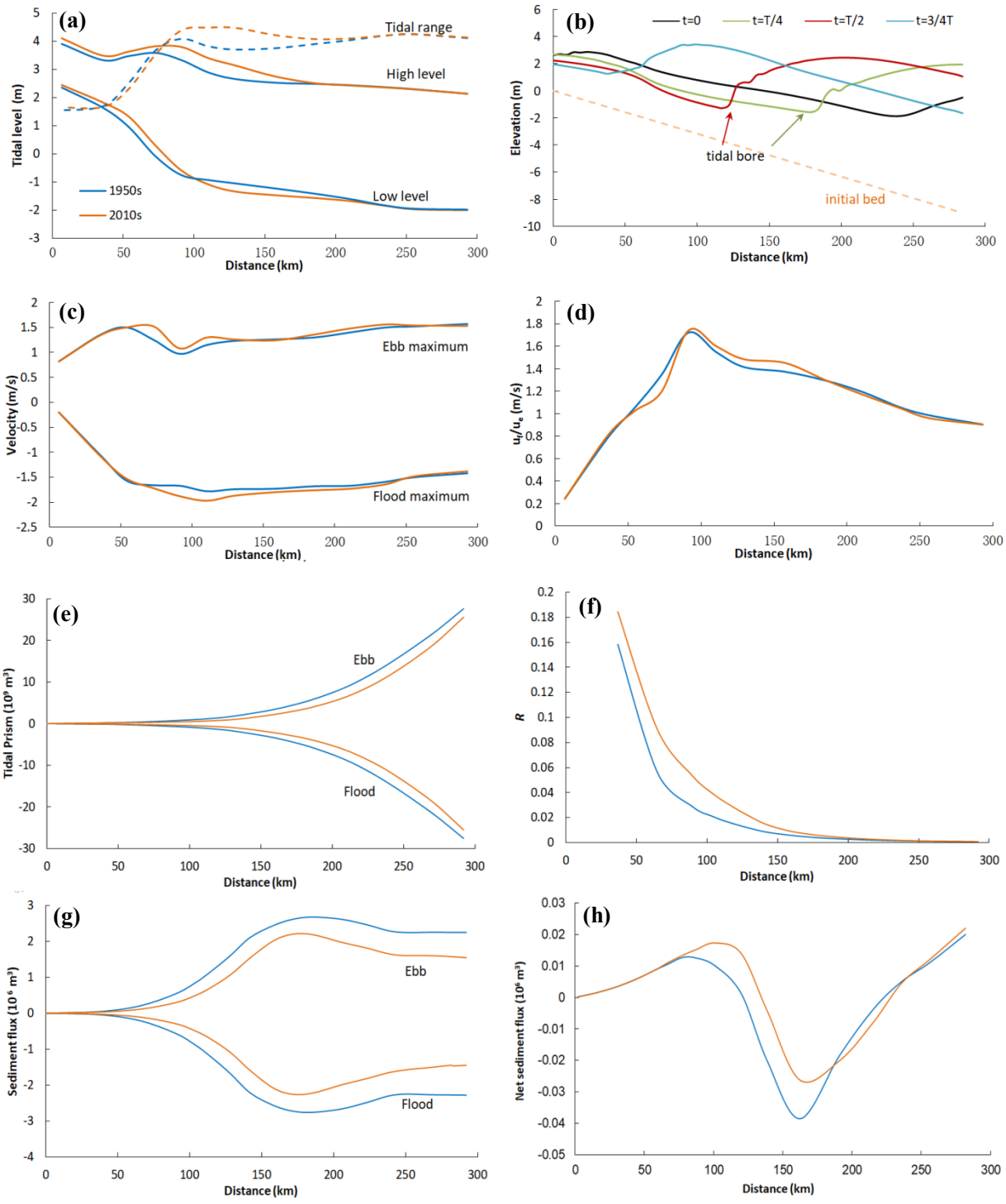

817

818 **Fig. 5.**

819

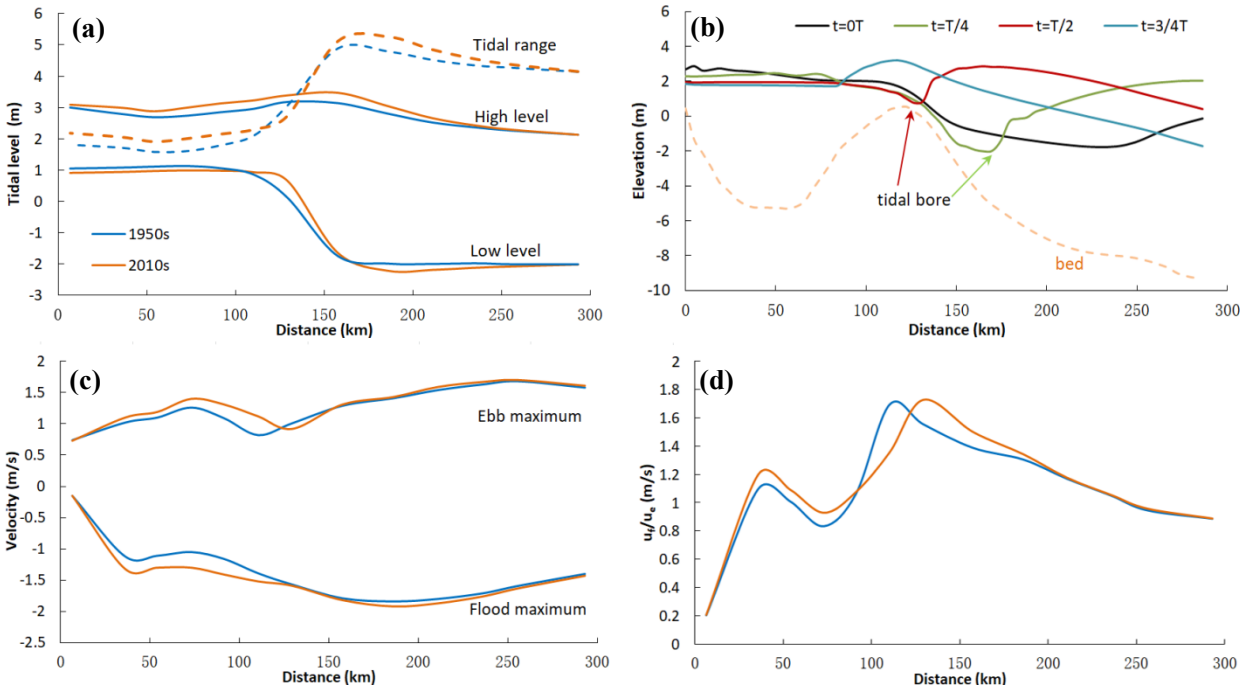

820

821

822 **Fig. 6.**

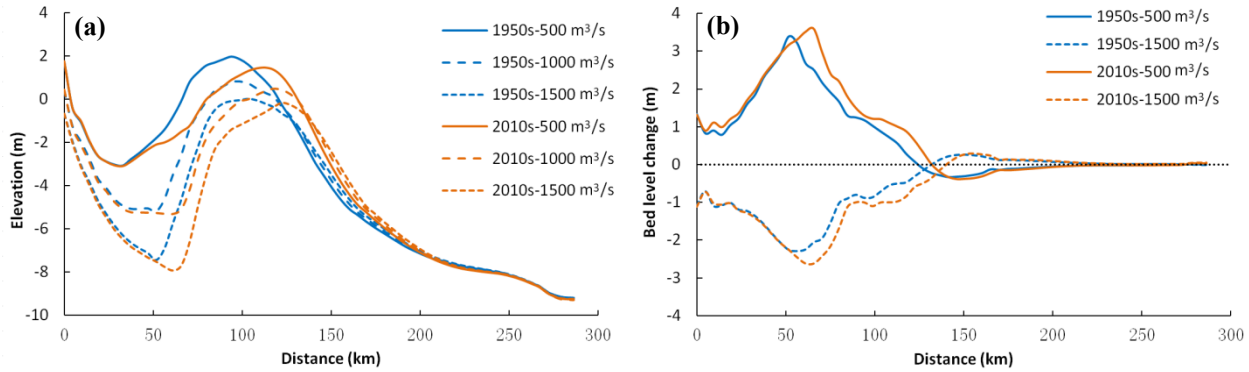
(a)
Elevation (m)
Distance (km)
1950s-500 m³/s
1950s-1000 m³/s
1950s-1500 m³/s
2010s-500 m³/s
2010s-1000 m³/s
2010s-1500 m³/s
(b)
Bed level change (m)
Distance (km)
1950s-500 m³/s
1950s-1500 m³/s
2010s-500 m³/s
2010s-1500 m³/s

823

824 **Fig. 7.**

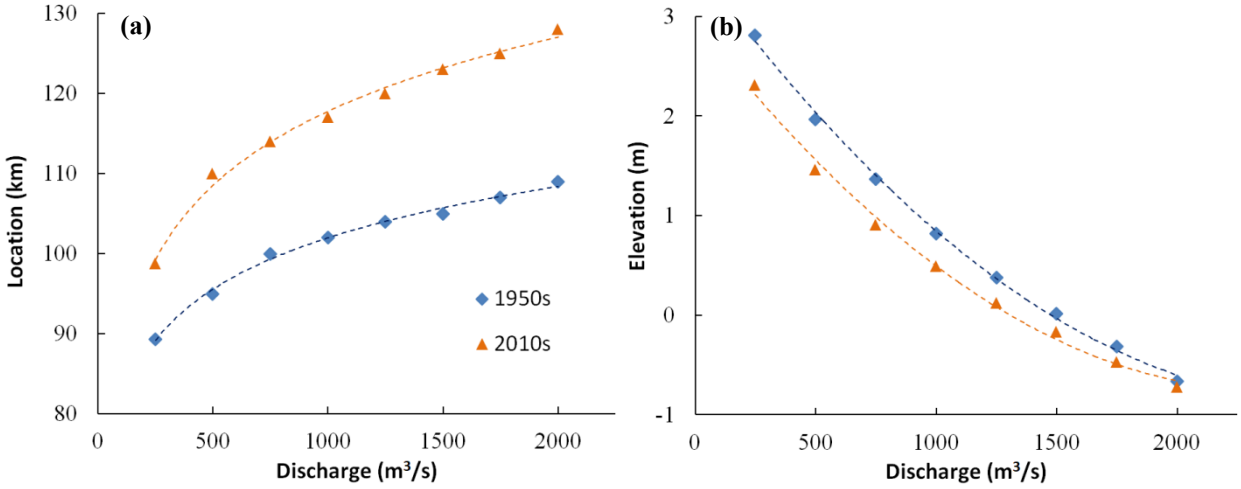
(a)
Location (km)
130
120
110
100
90
80
0
500
1000
1500
2000
Discharge (m³/s)
1950s
2010s
(b)
Elevation (m)
3
2
1
0
-1
0
500
1000
1500
2000
Discharge (m³/s)

825

826 **Fig. 8.**

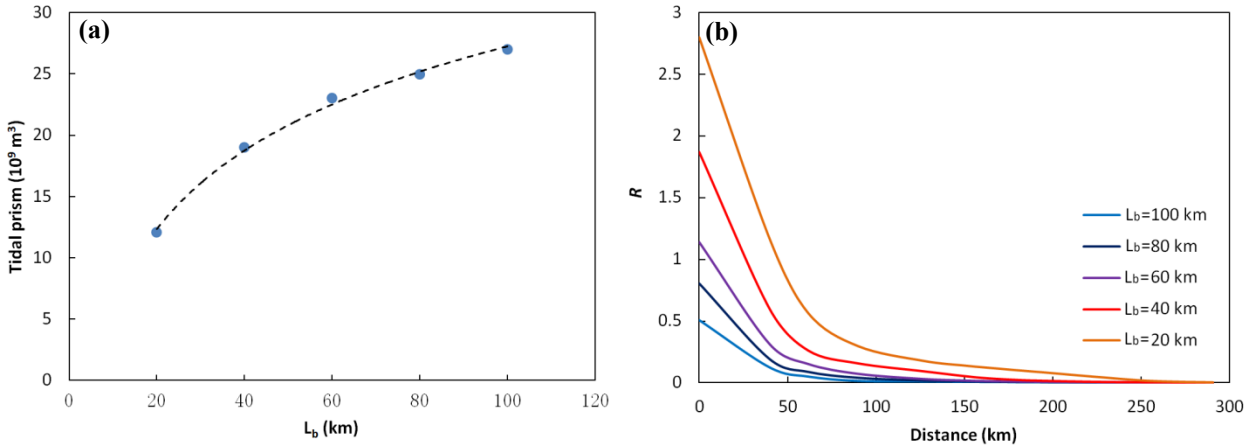
(a)
Tidal prism (10^9 m^3)
L_b (km)
(b)
R
Distance (km)
Lb=100 km
Lb=80 km
Lb=60 km
Lb=40 km
Lb=20 km

827

828 **Fig. 9.**

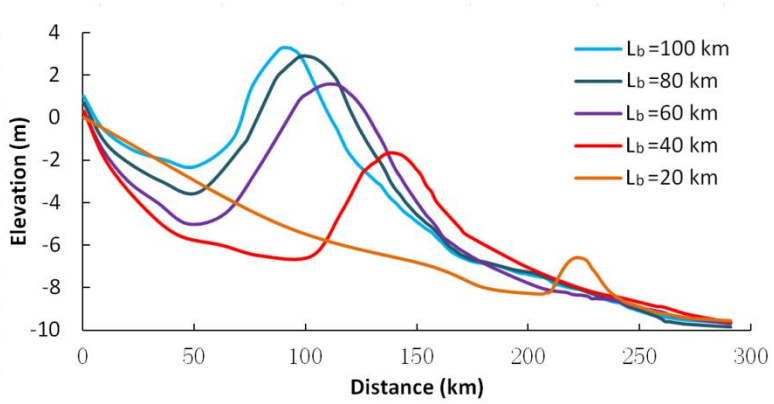

829

830 **Fig. 10.**

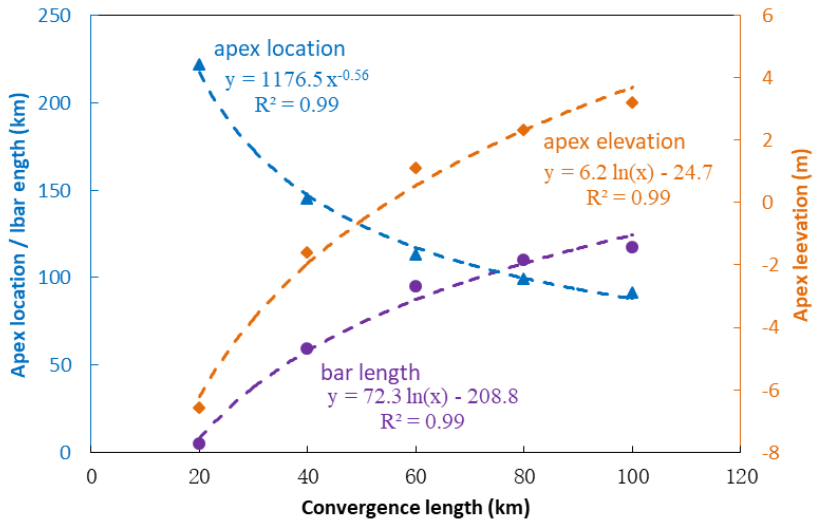

831

832 **Fig. 11.**

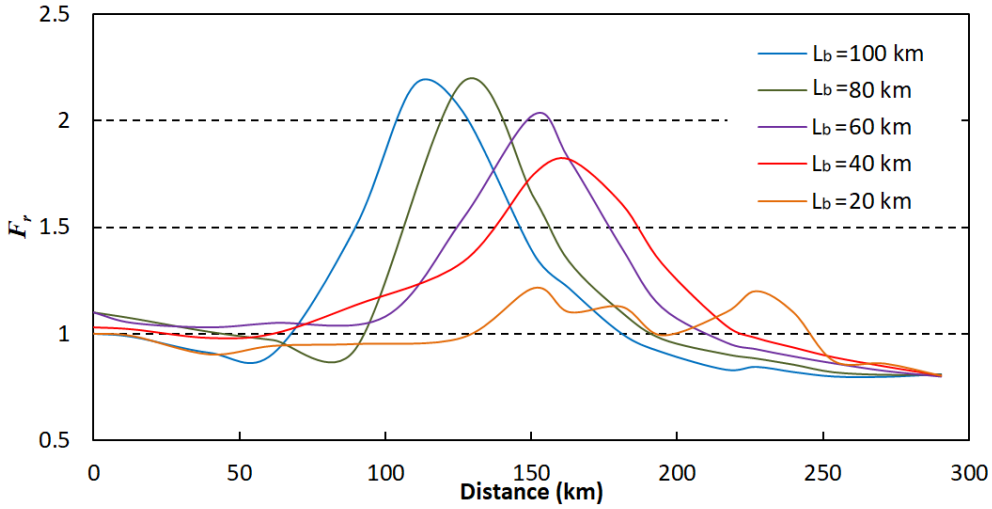
2.5
2
1.5
1
0.5
F_r
0
50
100
150
200
250
300
Distance (km)
Lb =100 km
Lb =80 km
Lb =60 km
Lb =40 km
Lb =20 km

Fig. 12.